First principle calculations of structural, electronic, thermodynamic and optical properties of $Pb_{1-x}Ca_xS$,$Pb_{1-x}Ca_xSe$ and $Pb_{1-x}Ca_xTe$ ternary alloys

2009 J. Phys.: Condens. Matter 21 195401

(http://iopscience.iop.org/0953-8984/21/19/195401)

J. Phys.: Condens. Matter **21** (2009) 195401 (9pp) doi:10.1088/0953-8984/21/19/195401

First principle calculations of structural, electronic, thermodynamic and optical properties of $Pb_{1-x}Ca_xS$, $Pb_{1-x}Ca_xSe$ and $Pb_{1-x}Ca_xTe$ ternary alloys

C Sifi[1], H Meradji[2], M Slimani[1], S Labidi[2], S Ghemid[2], E B Hanneche[1] and F El Haj Hassan[3,4]

[1] Laboratoire LESIMS, Département de Physique, Faculté des Sciences, Université de Annaba, Algeria
[2] Laboratoire de Physique des Rayonnements, Département de Physique, Faculté des Sciences, Université de Annaba, Algeria
[3] Faculté des Sciences (1), Laboratoire de Physique des Matériaux, Université Libanaise, Elhadath, Beirut, Lebanon

E-mail: hassan.f@ul.edu.lb

Received 25 December 2008, in final form 17 February 2009
Published 7 April 2009
Online at stacks.iop.org/JPhysCM/21/195401

Abstract
Using first principles total energy calculations within the full potential linearized augmented plane wave (FP-LAPW) method, we have investigated the structural, electronic, thermodynamic and optical properties of $Pb_{1-x}Ca_xS$, $Pb_{1-x}Ca_xSe$ and $Pb_{1-x}Ca_xTe$ ternary alloys. The effect of composition on lattice parameter, bulk modulus, band gap, refractive index and dielectric function was investigated. Deviations of the lattice constants from Vegard's law and the bulk modulus from linear concentration dependence were observed for the three alloys. Using the approach of Zunger and co-workers, the microscopic origins of band gap bowing have been detailed and explained. The disorder parameter (gap bowing) was found to be mainly caused by the chemical charge transfer effect. On the other hand, the thermodynamic stability of these alloys was investigated by calculating the excess enthalpy of mixing, ΔH_m, as well as the phase diagram. It was shown that all of these alloys are stable at low temperature. The calculated refractive indices and optical dielectric constants were found to vary nonlinearly with Ca composition.

1. Introduction

Lead chalcogenide solid solution semiconductors are expected to be applied to tunable laser diodes which operate in the mid-infrared wavelength region around 3 μm. In this study, band gap II–VI compounds are promising for wavelength optoelectronic applications in laser diodes and in light emitting diodes. They are considered to be mainly utilized in advanced measurement systems for detecting hydrocarbon pollutants in the air [1] and in a new optical fiber communication system over super-long distances; which has not yet been developed [2]. In order to use this laser diode, it is required to operate it close to room temperature. So far, many efforts have been made to fabricate such laser diodes [3–6], but this has not yet been realized. Semiconductor alloys, which are solid solutions of two or more semiconducting elements, have important technological applications, especially in the manufacture of electronic and electro-optical devices [7]. One of the easiest ways to artificially change the electronic and optical properties of semiconductors is by forming their alloys. It is possible to combine two different compounds with different optical band gaps and different rigidities in order to obtain a new material with intermediate properties.

Several studies have been devoted to the lead chalcogenides PbS, PbSe and PbTe and their structural, electronic

[4] Author to whom any correspondence should be addressed.

and optical properties [8–10], but no experimental or theoretical data have been reported yet on their alloys. The compositional variation in $Pb_{1-x}Ca_xS$, $Pb_{1-x}Ca_xSe$ and $Pb_{1-x}Ca_xTe$ alloys induces significant changes in their physical properties, such as electronic band structures and lattice parameters. The possible development of heterostructures based on these new material systems needs a detailed investigation of these alloys. Hence, in order to exploit these materials fully for new optical devices, the structural, electronic, thermodynamic and optical properties of these alloys need to be investigated in more detail. Motivated by the above considerations, we have carried out a study of the alloys of interest using the full potential linearized augmented plane wave (FP-LAPW) method. The alloys studied crystallize in the cubic phase over the whole range of composition x ($0 \leqslant x \leqslant 1$). The physical origins of gap bowing are investigated by following the approach of Zunger and co-workers [11]. This model is capable of taking into account the dominant effects of both chemical and bond length variations, unlike traditional methods like the VCA. In this approach, the alloy is studied in an ordered structure (we used a cubic supercell of eight atoms) designed to reproduce the most important pair correlation functions of a random (disorder) alloy and where the chemical and structural effects are captured very well.

The optoelectronic properties of the semiconductors alloys are essential for the design and fabrication of devices, the refractive indices and the optical dielectric constants of the materials have to be known as a function of composition.

The organization of this paper is as follows. We describe the FP-LAPW computational details in section 2. In section 3, results and discussion for structural, electronic, thermodynamic and optical properties are presented. Finally the conclusion is given in section 4.

2. Computational methods

The calculations were performed by the full potential linearized augmented plane (FP-LAPW) method to solve the Kohn–Sham equations as implemented in the WIEN2K code [12]. The exchange–correlation contribution was described within the generalized gradient approximation (GGA) proposed by Perdew *et al* [13] to calculate the total energy, while for the electronic properties, in addition to the GGA correction, Engel–Vosko's (EVGGA) formalism [14] was also applied. The core states of Pb, Ca, S, Se and Te atoms were treated self-consistently and fully relativistically relaxed in a spherical approximation, while the valence states were treated self-consistently within the semi-relativistic approximation. Unfortunately, this approximation breaks down for the heavy p-electron materials, such as Pb, and this can affect the results, especially the gap energy for small x, so we have to use a scissors operator. The best solution is also to apply a fully-relativistic treatment of the valence bands, which is not available in this code. Wavefunctions, charge density and potential were expanded inside muffin-tin spheres of radius R_{MT} by using spherical harmonics expansion, while in the remaining space of the unit cell a plane wave basis set was chosen. The plane wave cutoff of $K_{max} = 8.0/R_{MT}$ (R_{MT} is the smallest muffin-tin radius) was used for the expansion of the wavefunction in the interstitial region for all three alloys and the six binary compounds CaS, CaSe, CaTe, PbS, PbSe and PbTe. The values of R_{MT} were assumed to be 1.9, 2.0, 2.1, 2.2 and 2.4 a.u. for Ca, S, Se, Pb and Te atoms, respectively. The charge density was Fourier expanded up to $G_{max} = 14$ $(Ryd)^{1/2}$. The maximal l value for the wavefunction expansion inside the atomic spheres was confined to $l_{max} = 10$. Meshes of 47 special k-points for binary compounds and 125 special k-points for alloys were used in the irreducible wedge of the Brillouin zone. Both the plane wave cutoff and the number of k-points were varied to ensure total energy convergence.

3. Results and discussion

3.1. Structural properties

In the present work we analyze the structural properties of the binary compounds PbS, PbSe, PbTe, CaS, CaSe, CaTe and their alloys. A rocksalt structure was assumed. The alloys were modeled at some selected compositions with ordered structures described in terms of periodically repeated supercells with eight atoms per unit cell, for the compositions $x = 0.25$, 0.5, 0.75. For the considered structures, we perform the structural optimization by minimizing the total energy with respect to the cell parameters and also the atomic positions. The calculated total energies at many different volumes around equilibrium were fitted by the Murnaghan equation of state [15] in order to obtain the equilibrium lattice constant and the bulk modulus for the binary compounds and their alloys. Our results for the materials of interest are compared with the available experimental and theoretical predictions in table 1. Considering the general trend that the GGA usually overestimates the lattice parameters [20], our GGA results for the binary compounds are in reasonable agreement with experimental values and other calculated values. Usually, in the treatment of alloy problems, it is assumed that the atoms are located at ideal lattice sites and the lattice constants of alloys should vary linearly with composition x according to Vegard's law [21]; however, violations of Vegard's rule have been reported in semiconductor alloys both experimentally [22] and theoretically [23].

The calculated lattice parameters at different compositions of $Pb_{1-x}Ca_xS$, $Pb_{1-x}Ca_xSe$ and $Pb_{1-x}Ca_xTe$ alloys exhibit a tendency to Vegard's law, with marginal upward bowing parameters equal to -0.016, -0.014 and -0.010 Å, respectively, obtained by fitting the calculated values with a polynomial function. This small deviation is due to the relaxation of Pb–S and Ca–S bond lengths in $Pb_{1-x}Ca_xS$, Pb–Se and Ca–Se bond lengths in $Pb_{1-x}Ca_xSe$ and Pb–Te and Ca–Te bond lengths in $Pb_{1-x}Ca_xTe$.

The composition dependence of the bulk modulus for $Pb_{1-x}Ca_xS$, $Pb_{1-x}Ca_xSe$ and $Pb_{1-x}Ca_xTe$ alloys is compared with the results predicted by linear concentration dependence (LCD). A small deviation from LCD is observed, with downward bowing equal to -0.54 GPa for the $Pb_{1-x}Ca_xS$ alloy and upward bowing equal to 0.01 GPa for the

Table 1. Calculated lattice parameter (a) and bulk modulus (B) of for $Pb_{1-x}Ca_xS$, $Pb_{1-x}Ca_xSe$ and $Pb_{1-x}Ca_xTe$ ternary alloys at equilibrium volume.

		Lattice constants a (Å)			Bulk modulus B (GPa)		
	x	This work	Experiment	Other calculations	This work	Experiment	Other calculations
$Pb_{1-x}Ca_xS$	1	5.722	5.69 [16]	5.717 [17]	57.10	64 [16]	57.42 [17]
	0.75	5.807			55.84		
	0.5	5.880			54.33		
	0.25	5.946			52.82		
	0	6.007	5.94 [19]	5.936 [18]	51.31		
$Pb_{1-x}Ca_xTe$	1	6.396	6.345 [16]	6.390 [17]	37.29	41.80 [16]	39.60 [17]
	0.75	6.446			37.47		
	0.5	6.492			37.66		
	0.25	6.532			37.85		
	0	6.567	6.462 [19]	6.34 [18]	38.04		
$Pb_{1-x}Ca_xSe$	1	5.964	5.910 [16]	5.968 [17]	47.52	51 [16]	48.75 [17]
	0.75	6.034			48.05		
	0.5	6.105			48.59		
	0.25	6.166			49.12		
	0	6.217	6.123 [19]	6.124 [18]	49.66		

$Pb_{1-x}Ca_xSe$ alloy, while in the case of $Pb_{1-x}Ca_xTe$ our calculations exhibit a good agreement with LCD, with a bowing parameter close to zero. This deviation is mainly due to the mismatch of the bulk modulus of binary compounds, which is in our case very small. It is clearly seen that the bulk modulus decreases on increasing the atomic number of the chalcogen atom. Hence, we conclude that PbTe and CaTe are more compressible compared the other calcium and lead chalcogenide compounds, respectively.

3.2. Electronic properties

The self-consistent scalar relativistic indirect band gaps of lead chalcogenide compounds and their alloys were calculated within the GGA and EVGGA schemes. The results for each compound are given in table 2. It is well known that the GGA usually underestimates the experimental energy band gap [24, 25]. This is mainly due to the fact that the functionals within this approximation have simple forms that are not sufficiently flexible to accurately reproduce both exchange–correlation energy and its charge derivative. Engel and Vosko by considering this underestimation constructed a new functional form of GGA which was able to better reproduce the exchange potential at the expense of less agreement as regards exchange energy when compared to experiment. This approach, which is called EVGGA, yields a better band splitting and some other properties which mainly depend on the accuracy of exchange–correlation potential. However, in this method, the quantities that depend on an accurate description of exchange energy E_x, such as equilibrium volumes and bulk modulus, are in poor agreement with experiment.

The band gap E_{gABC} of an alloy such as $A_xB_{1-x}C_x$ is not given by the linear concentration x weighted average of the AC (E_{gAC}) and BC (E_{gBC}) gaps but has a quadratic form, $E_{gABC} = xE_{gAC} + (1-x)E_{gBC} - bx(1-x)$, where b is known as the bowing parameter. The band gap of alloys in various device applications has provoked an interest in computing the optical band gap bowing in terms of the constituent elements AC and BC.

Table 2. Gap energy E_g of $Pb_{1-x}Ca_xS$, $Pb_{1-x}Ca_xSe$ and $Pb_{1-x}Ca_xTe$ ternary alloys at equilibrium volume.

		Band gap E_g	
		This work	
	x	GGA	EVGGA
$Pb_{1-x}Ca_xS$	1	2.405	3.176
	0.75	1.195	1.883
	0.5	0.764	1.441
	0.25	0.458	1.216
	0	0.486	1.221
$Pb_{1-x}Ca_xSe$	1	2.105	2.815
	0.75	1.162	1.598
	0.5	0.739	1.312
	0.25	0.440	1.092
	0	0.423	1.079
$Pb_{1-x}Ca_xTe$	1	1.582	2.228
	0.75	1.310	1.575
	0.5	1.073	1.484
	0.25	0.871	1.389
	0	0.819	1.331

In order to better understand the physical origins of the gap bowing of alloys, we follow the procedure of Bernard and Zunger [26] in which the bowing parameter b is decomposed into three physically distinct contributions. By considering the fact that the bowing dependence on the composition is marginal, the authors limited their calculations to $x = 0.5$ (50%–50% alloy). The overall gap bowing coefficient at $x = 0.5$ measures the change in band gap according to the reaction:

$$AB(a_{AB}) + AC(a_{AC}) \rightarrow AB_{0.5}C_{0.5}(a_{eq}) \qquad (1)$$

where a_{AB} and a_{AC} are the equilibrium lattice constants of the binary compounds AB and AC, respectively, and a_{eq} is the alloy equilibrium lattice constant. We now decompose reaction (1) into three steps:

$$AB(a_{AB}) + AC(a_{AC}) \xrightarrow{VD} AB(a) + AC(a), \qquad (2)$$

$$\mathrm{AB}(a) + \mathrm{AC}(a) \xrightarrow{\mathrm{CE}} \mathrm{AB_{0.5}C_{0.5}}(a), \quad (3)$$

$$\mathrm{AB_{0.5}C_{0.5}}(a) \xrightarrow{\mathrm{SR}} \mathrm{AB_{0.5}C_{0.5}}(a_{\mathrm{eq}}). \quad (4)$$

The first step measures the volume deformation (VD) effect on the bowing. The corresponding contribution to the total gap bowing parameter b_{VD} represents the relative response of the band structure of the binary compounds AB and AC to hydrostatic pressure, which here arises from the change of their individual equilibrium lattice constants to the alloy value $a = a(x)$ (from Vegard's rule). The second contribution, the charge exchange (CE) contribution b_{CE}, reflects a charge transfer effect which is due to the different (averaged) bonding behavior at the lattice constant a. The final step measures changes upon passing from the unrelaxed to the relaxed alloy by b_{SR}. Consequently, the total gap bowing parameter is defined as

$$b = b_{\mathrm{VD}} + b_{\mathrm{CE}} + b_{\mathrm{SR}}, \quad (5)$$

$$b_{\mathrm{VD}} = 2[\varepsilon_{\mathrm{AB}}(a_{\mathrm{AB}}) - \varepsilon_{\mathrm{AB}}(a) + \varepsilon_{\mathrm{AC}}(a_{\mathrm{AC}}) - \varepsilon_{\mathrm{AC}}(a)], \quad (6)$$

$$b_{\mathrm{CE}} = 2[\varepsilon_{\mathrm{AB}}(a) + \varepsilon_{\mathrm{AC}}(a) - 2\varepsilon_{\mathrm{ABC}}(a)], \quad (7)$$

$$b_{\mathrm{SR}} = 4[\varepsilon_{\mathrm{ABC}}(a) - \varepsilon_{\mathrm{ABC}}(a_{\mathrm{eq}})], \quad (8)$$

where ε is the energy gap that has been calculated for the indicated atomic structures and lattice constants. All the terms in equations (6)–(8) are calculated separately via self-consistent band structure calculations within density functional theory and the results are given in table 3. The total gap bowing for all the three alloys were found to be mainly caused by the charge transfer contribution b_{CE}. It is due to the large electronegativity difference between atoms. Indeed, the significant role of b_{CE} is correlated with the ionicity factor difference among constituent binary compounds PbS ($f_{\mathrm{i}} = 0.115$), CaS ($f_{\mathrm{i}} = 0.430$), PbTe ($f_{\mathrm{i}} = 0.022$), CaTe ($f_{\mathrm{i}} = 0.260$), PbSe ($f_{\mathrm{i}} = 0.086$) and CaSe ($f_{\mathrm{i}} = 0.380$). These values are calculated using the Pauling scale [27]. The volume deformation term b_{VD} contributes to the bowing parameter at smaller magnitude. The weak contributions of b_{VD} can be correlated to the small mismatch of the lattice constants of the corresponding binary compounds. The contribution of the structural relaxation b_{SR} is small in the three alloys. Finally, it is clearly seen that our EVGGA values for bowing parameters are larger than the corresponding values within GGA.

Alternatively, we calculated the total bowing parameter by fitting the nonlinear variation of the calculated band gaps versus concentration with quadratic functions. The results are shown in figures 1(a)–(c) and obey the following variations:

$$\mathrm{Pb_{1-x}Ca_xS} \Rightarrow \begin{cases} E_{\mathrm{g}}^{\mathrm{GGA}} = 0.518 - 1.142x + 2.972x^2 \\ E_{\mathrm{g}}^{\mathrm{EVGGA}} = 1.274 - 1.384x + 3.215x^2 \end{cases} \quad (9)$$

$$\mathrm{Pb_{1-x}Ca_xSe} \Rightarrow \begin{cases} E_{\mathrm{g}}^{\mathrm{GGA}} = 0.439 - 0.624x + 2.258x^2 \\ E_{\mathrm{g}}^{\mathrm{EVGGA}} = 1.137 - 1.236x + 2.826x^2 \end{cases} \quad (10)$$

$$\mathrm{Pb_{1-x}Ca_xTe} \Rightarrow \begin{cases} E_{\mathrm{g}}^{\mathrm{GGA}} = 0.806 + 0.243x + 0.542x^2 \\ E_{\mathrm{g}}^{\mathrm{EVGGA}} = 1.375 - 0.563x + 1.355x^2. \end{cases} \quad (11)$$

We note that the calculated quadratic parameters (gap bowing) within GGA and EVGGA are close to their corresponding results obtained by Zunger approach.

Table 3. Decomposition of the optical bowing into volume deformation (VD), charge exchange (CE), and structural relaxation (SR) contributions compared with that obtained by a quadratic fit (all values are in eV).

		This work (Zunger)		Quadratic equation	
		GGA	EVGGA	GGA	EVGGA
$\mathrm{Pb_{1-x}Ca_xS}$	b_{VD}	0.240	0.286		
	b_{CE}	2.577	2.851		
	b_{SR}	−0.093	−0.110		
	b	2.724	3.027	2.972	3.214
$\mathrm{Pb_{1-x}Ca_xSe}$	b_{VD}	0.141	0.194		
	b_{CE}	2.046	2.427		
	b_{SR}	−0.089	−0.082		
	b	2.098	2.539	2.256	2.827
$\mathrm{Pb_{1-x}Ca_xTe}$	b_{VD}	0.057	0.070		
	b_{CE}	0.535	1.205		
	b_{SR}	−0.084	−0.094		
	b	0.508	1.181	0.541	1.355

3.3. Thermodynamic properties

Focusing on the thermodynamic properties of $\mathrm{Pb_{1-x}Ca_xS}$, $\mathrm{Pb_{1-x}Ca_xSe}$ and $\mathrm{Pb_{1-x}Ca_xTe}$ alloys, we calculated the phase diagram based on the regular-solution model [28–30]. The Gibbs free energy of mixing, ΔG_{m} for alloys is expressed as

$$\Delta G_{\mathrm{m}} = \Delta H_{\mathrm{m}} - T\Delta S_{\mathrm{m}}, \quad (12)$$

where

$$\Delta H_{\mathrm{m}} = \Omega x(1-x) \quad (13)$$

$$\Delta S_{\mathrm{m}} = -R[x\ln x + (1-x)\ln(1-x)] \quad (14)$$

ΔH_{m} and ΔS_{m} being the enthalpy and the entropy of mixing, respectively; Ω is the interaction parameter, R is the gas constant and T is the absolute temperature. Only the interaction parameter Ω depends on the material.

The mixing enthalpy of alloys can be obtained from the calculated total energies as $\Delta H_{\mathrm{m}} = E_{\mathrm{AB_xC_{1-x}}} - xE_{\mathrm{AB}} - (1-x)E_{\mathrm{AC}}$, where $E_{\mathrm{AB_xC_{1-x}}}$, E_{AB} and E_{AC} are the respective energies of $\mathrm{AB_xC_{1-x}}$ alloy and the binary compounds AB and AC. We then calculated ΔH_{m} to obtain Ω as a function of concentration. The interaction parameter increases almost linearly with increasing x. From a linear fit we obtained

$$\mathrm{Pb_{1-x}Ca_xS} \Rightarrow \Omega\,(\mathrm{kcal\ mol^{-1}}) = 0.5134x + 1.419 \quad (15)$$

$$\mathrm{Pb_{1-x}Ca_xSe} \Rightarrow \Omega\,(\mathrm{kcal\ mol^{-1}}) = 0.568x + 1.022 \quad (16)$$

$$\mathrm{Pb_{1-x}Ca_xTe} \Rightarrow \Omega\,(\mathrm{kcal\ mol^{-1}}) = 0.247x + 0.686. \quad (17)$$

The average values of the x-dependent Ω in the range $0 \leqslant x \leqslant 1$ obtained from these equations for $\mathrm{Pb_{1-x}Ca_xS}$, $\mathrm{Pb_{1-x}Ca_xSe}$ and $\mathrm{Pb_{1-x}Ca_xTe}$ alloys are 1.676, 1.306 and 0.809 kcal mol^{-1}, respectively.

Now, we first calculate ΔG_{m} by using equations (12)–(14). Then we use the Gibbs free energy at different concentrations to calculate the T–x phase diagram which shows the stable, metastable, and unstable mixing regions of the alloy. At a temperature lower than the critical temperature T_{c} the two binodal points are determined as

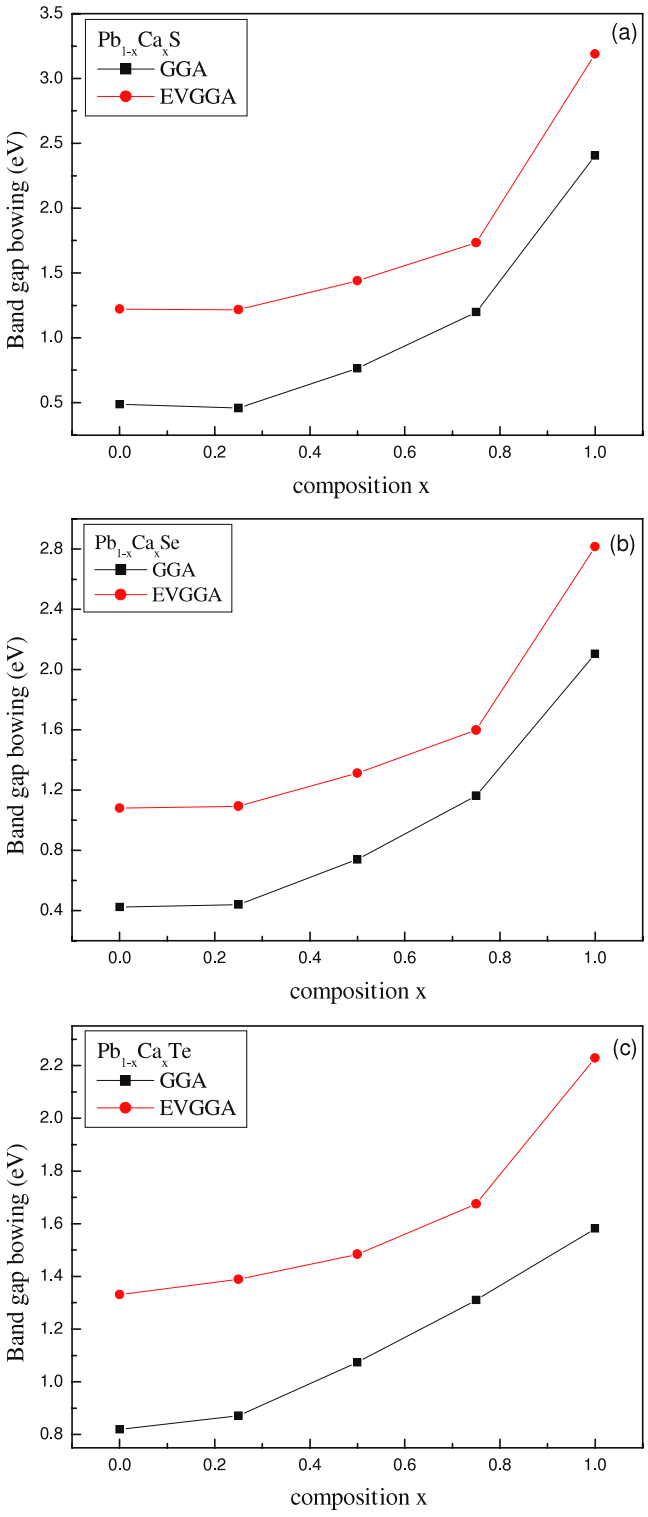

Figure 1. Composition dependence of calculated band gap using GGA (solid squares) and EVGGA (solid circles) for (a) $Pb_{1-x}Ca_xS$, (b) $Pb_{1-x}Ca_xSe$, (c) $Pb_{1-x}Ca_xTe$ alloys.

(This figure is in colour only in the electronic version)

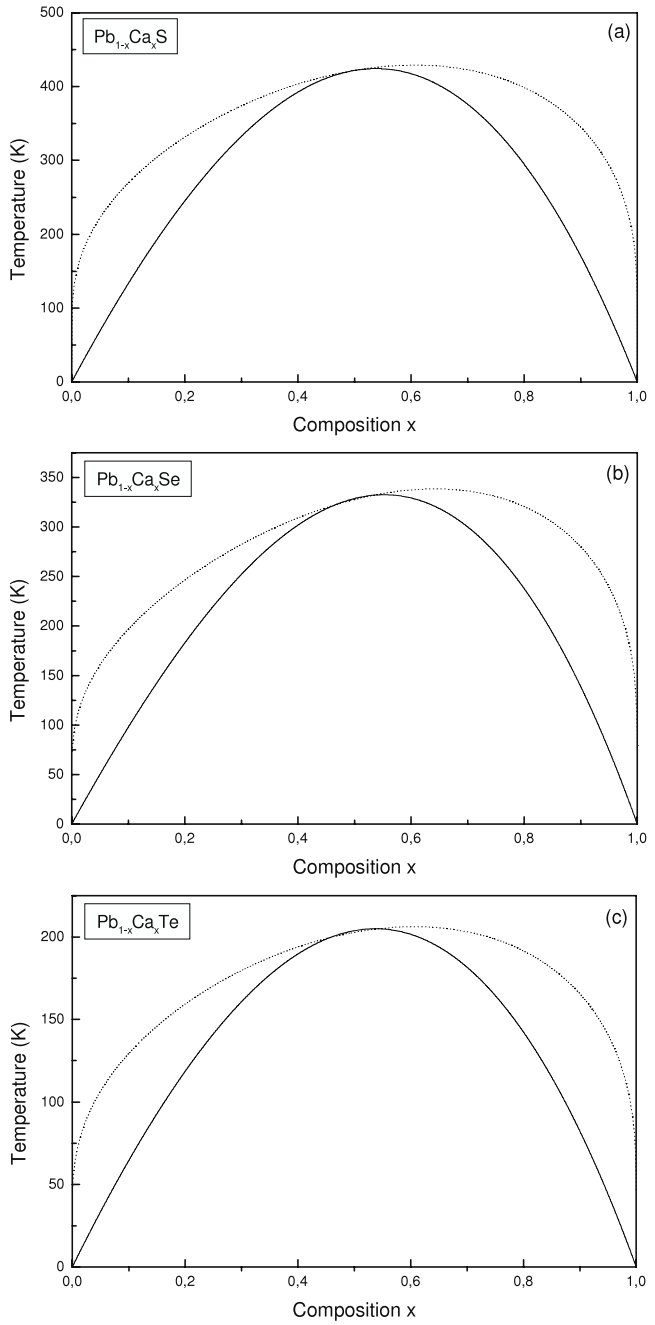

Figure 2. T–x phase diagram of (a) $Pb_{1-x}Ca_xS$, (b) $Pb_{1-x}Ca_xSe$, (c) $Pb_{1-x}Ca_xTe$ alloys. Dashed line: binodal curve; solid line: spinodal curve.

those points at which the common tangent line touches the ΔG_m curves. The two spinodal points are determined as those points at which the second derivative of ΔG_m is zero; $\partial^2(\Delta G_m)/\partial x^2 = 0$.

Figure 2 shows the calculated phase diagrams including the spinodal and binodal curves of the alloys of interest. We observed a critical temperature T_c of 425, 328 and 204 K for $Pb_{1-x}Ca_xS$, $Pb_{1-x}Ca_xSe$ and $Pb_{1-x}Ca_xTe$ alloys, respectively. We have calculated the phase diagram by using the linear equations of the x-dependent Ω. Hence the phase diagram looks asymmetric about $x = 0.5$ due to the asymmetry of ΔH_m.

The spinodal curve in the phase diagram marks the equilibrium solubility limit, i.e., the miscibility gap. For temperatures and compositions above this curve a

Table 4. Refractive indices of $Pb_{1-x}Ca_xS$, $Pb_{1-x}Ca_xSe$ and $Pb_{1-x}Ca_xTe$ for different compositions x.

		This work				
		FP-LAPW	Relation (21)	Relation (22)	Relation (23)	Experiment
$Pb_{1-x}Ca_xS$	0	3.87	3.861	3.640	3.783	4.55 [34]
	0.25	3.56	3.918	3.664	3.710	
	0.5	3.18	3.448	3.415	3.611	
	0.75	2.77	3.083	3.124	3.343	
	1	2.30	2.588	2.547	2.592	2.05 [35]
$Pb_{1-x}Ca_xSe$	0	3.22	3.997	3.695	3.822	4.70 [34]
	0.25	3.81	3.957	3.680	3.811	
	0.5	3.21	3.476	3.434	3.625	
	0.75	2.80	3.105	3.144	3.364	
	1	2.35	2.676	2.665	2.779	2.09 [35]
$Pb_{1-x}Ca_xTe$	0	4.67	3.389	3.375	3.576	5.64 [34]
	0.25	4.34	3.336	3.337	3.544	
	0.5	3.54	3.167	3.200	3.418	
	0.75	3.10	3.013	3.056	3.272	
	1	2.57	2.875	2.907	3.103	2.17 [35]

homogeneous alloy is predict. The wide range between spinodal and binodal curves indicates that the alloy may exist as a metastable phase. Finally, our results indicate that the chalcogenide alloys are stable at low temperatures and show a broad miscibility gap surrounded by the binodal line.

3.4. Optical properties

The optical properties of matter can be described by the complex dielectric function $\varepsilon(\omega)$, which represents the linear response of a system due to an external electromagnetic field with a small wavevector. It can be expressed as

$$\varepsilon(\omega) = \varepsilon_1(\omega) + i\varepsilon_2(\omega), \tag{18}$$

where ε_1 and ε_2 are the real and imaginary components of the dielectric function, respectively. To calculate such parameters the band gap is needed. It is well known that energy gaps are systematically underestimated in *ab initio* calculations and that this is an intrinsic feature of density functional theory, hence to calculate the joint density of states we have to do an energy shift by using a scissors operator which is the difference between experimental results and our work. The imaginary part of the dielectric function in the long wavelength limit has been obtained directly from the electronic structure calculation, using the joint density of states and the optical matrix elements. The real part of the dielectric function can be derived from the imaginary part by the Kramers–Kronig relationship. The knowledge of both the real and imaginary parts of the dielectric function allows the calculation of important optical functions. The refractive index $n(\omega)$ is given by

$$n(\omega) = \left[\frac{\varepsilon_1(\omega)}{2} + \frac{\sqrt{\varepsilon_1^2(\omega) + \varepsilon_2^2(\omega)}}{2}\right]^{1/2}. \tag{19}$$

At low frequency ($\omega = 0$), we get the following relation:

$$n(0) = \varepsilon^{1/2}(0). \tag{20}$$

The refractive index and optical dielectric constants are very important in determining the optical and electric properties of the crystal. Advanced applications of these alloys can significantly benefit from accurate index data. The use of fast non-destructive optical techniques for epitaxial layer characterization (determination of thickness or alloy composition) is limited by the accuracy with which refractive indices can be related to alloy composition. These applications require an analytical expression of known accuracy to relate the wavelength dependence of refractive index to alloy composition, as determined from simple techniques as photoluminescence. A few empirical relations [31–33] relate the refractive index to the energy band gap for a large set of semiconductors. However, in these relations the refractive index n is independent of the temperature and the incident-photon energy. The following models are used:

(i) The Moss formula [31] based on an atomic model

$$E_g n^4 = k, \tag{21}$$

where E_g is the energy band gap and k a constant. The value of k is given to be 108 eV by Ravindra and Srivastava [31].

(ii) The expression proposed by Ravindra *et al* [32]

$$n = \alpha + \beta E_g \tag{22}$$

with $\alpha = 4.084$; and $\beta = -0.62\ \text{eV}^{-1}$.

(iii) Herve and Vandamme's empirical relation [33] is given by

$$n = \sqrt{1 + \left(\frac{A}{E_g + B}\right)^2} \tag{23}$$

with $A = 13.6$ eV and $B = 3.4$ eV.

Table 4 lists the values of the refractive index for the alloys under investigation for some compositions, x, obtained from FP-LAPW calculations and the different models. Comparison with the experimental data has been made where possible. One can note that the values obtained for the refractive index of binary compounds within the FP-LAPW method

are in better agreement with available experimental results in comparison with the values calculated by the empirical relations. Unfortunately, no comparison has been made for the refractive index of the alloys of interest in the $0 < x < 1$ composition range, as there are no known available data to the best of our knowledge.

Using the expressions (20)–(23), the variation of the refractive index for the three alloys of interest as a function of the Ca concentration x has been studied. Our results are plotted in figures 3(a)–(c), and one can notice that the refractive index decreases with increasing Ca content. Accordingly, a nonlinear behavior of refractive index can be clearly noticed, which arises from the effect of compositional disorder. The calculated refractive indices versus concentration were fitted by a polynomial equation. The results are summarized as follows:

$$\mathrm{Pb}_{1-x}\mathrm{Ca}_x\mathrm{S} \Rightarrow \begin{cases} n_1(x) = 3.913 - 0.211x - 1.142x^2 \\ \quad \text{(from relation (21))}, \\ n_2(x) = 3.645 + 0.331x - 1.422x^2 \\ \quad \text{(from relation (22))}, \\ n_3(x) = 3.739 + 0.643x - 1.743x^2 \\ \quad \text{(from relation (23))}, \\ n_4(x) = 3.872 - 1.172x - 0.400x^2 \\ \quad \text{(FP-LAPW)}. \end{cases} \tag{24}$$

$$\mathrm{Pb}_{1-x}\mathrm{Ca}_x\mathrm{Se} \Rightarrow \begin{cases} n_1(x) = 4.045 - 0.634x - 0.763x^2 \\ \quad \text{(from relation (21))}, \\ n_2(x) = 3.704 + 0.072x - 1.111x^2 \\ \quad \text{(from relation (22))}, \\ n_3(x) = 3.812 + 0.384x - 1.398x^2 \\ \quad \text{(from relation (23))}, \\ n_4(x) = 3.3582 - 1.06x - 2.16x^2 \\ \quad \text{(FP-LAPW)}. \end{cases} \tag{25}$$

$$\mathrm{Pb}_{1-x}\mathrm{Ca}_x\mathrm{Te} \Rightarrow \begin{cases} n_1(x) = 3.404 - 0.363x - 0.177x^2 \\ \quad \text{(from relation (21))}, \\ n_2(x) = 3.386 - 0.225x - 0.262x^2 \\ \quad \text{(from relation (22))}, \\ n_3(x) = 3.584 - 0.151x - 0.336x^2 \\ \quad \text{(from relation (23))}, \\ n_4(x) = 4.726 - 2.130x - 0.046x^2 \\ \quad \text{(FP-LAPW)}. \end{cases} \tag{26}$$

For $\mathrm{Pb}_{1-x}\mathrm{Ca}_x\mathrm{S}$ and $\mathrm{Pb}_{1-x}\mathrm{Ca}_x\mathrm{Te}$ alloys, a weak upward bowing is observed for $n_4(x)$, compared with the other ones, while for $\mathrm{Pb}_{1-x}\mathrm{Ca}_x\mathrm{Se}$ alloy, it has a contrary behavior to both others. For this alloy a significant upward bowing is observed for $n_4(x)$. From these equations, we can note the strong nonlinear dependence of the refractive index of the alloys with concentration x. Interestingly, we note that on going from lead chalcogenides (PbS, PbSe and PbTe) to calcium chalcogenides

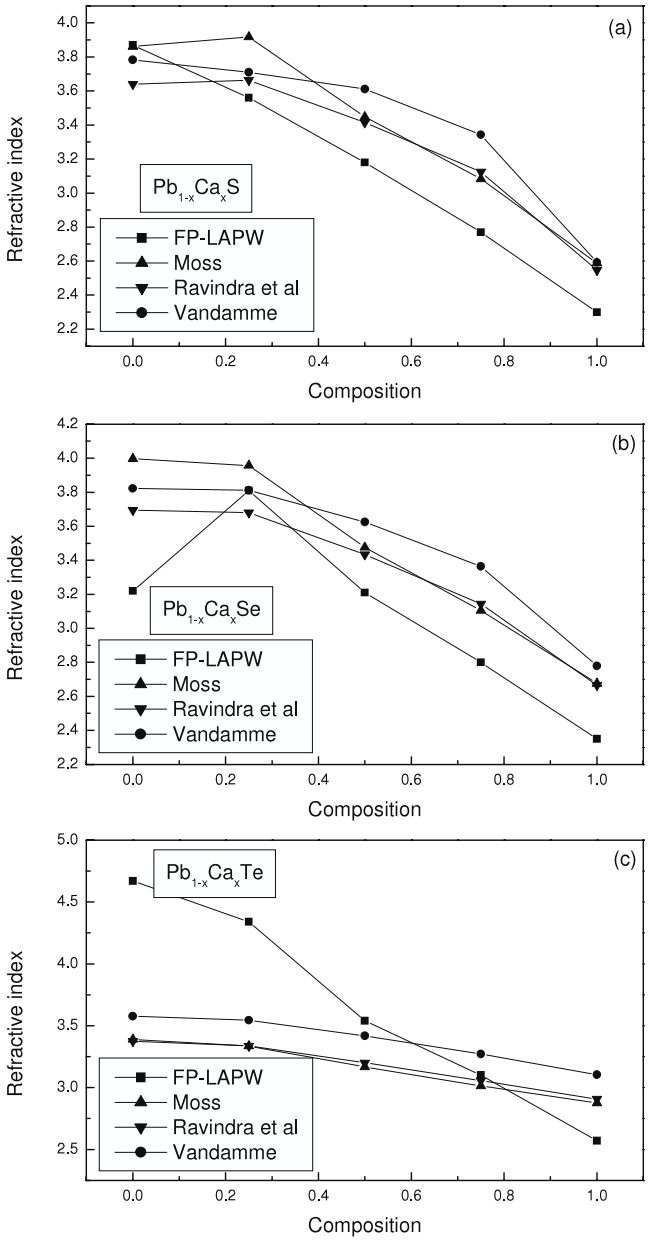

Figure 3. Refractive index for (a) $\mathrm{Pb}_{1-x}\mathrm{Ca}_x\mathrm{S}$, (b) $\mathrm{Pb}_{1-x}\mathrm{Ca}_x\mathrm{Se}$ and (c) $\mathrm{Pb}_{1-x}\mathrm{Ca}_x\mathrm{Te}$ alloys for different composition x.

(CaS, CaSe and CaTe), the band gap of the three alloys decreases (see figure 1), whereas the refractive index increases. The ternary alloys show that the smaller band gap material has a large value of the refractive index as is the general behavior of many other groups III–V semiconductors alloys [36]. The optical dielectric constant bas been directly deduced from the relation (20). Qualitatively, the compositional dependence of the dielectric function of the alloys has the same trend as that of the refractive index. This is expected since our results are related to the refractive index discussed previously in the present work. It also seems that the FP-LAPW method leads to the obtention of values for ε that are closer to experiment than the other used models. Least-squares fit were made on

our data:

$$\mathrm{Pb}_{1-x}\mathrm{Ca}_x\mathrm{S} \Rightarrow \begin{cases} \varepsilon_1(x) = 15.347 - 2.710x - 6.195x^2 \\ \quad \text{(from relation (21))} \\ \varepsilon_2(x) = 13.349 + 1.164x - 8.0.48x^2 \\ \quad \text{(from relation (22))} \\ \varepsilon_3(x) = 14.076 + 3.128x - 10.238x^2 \\ \quad \text{(from relation (23))} \\ \varepsilon_4(x) = 15.031 - 9.706x - 0.042x^2 \\ \quad \text{(FP-LAPW)} \end{cases} \tag{27}$$

$$\mathrm{Pb}_{1-x}\mathrm{Ca}_x\mathrm{Se} \Rightarrow \begin{cases} \varepsilon_1(x) = 16.377 - 5.813x - 3.645x^2 \\ \quad \text{(from relation (21))} \\ \varepsilon_2(x) = 13.760 - 0.418x - 6.285x^2 \\ \quad \text{(from relation (22))} \\ \varepsilon_3(x) = 14.591 + 1.736x - 8.5268x^2 \\ \quad \text{(from relation (23))} \\ \varepsilon_4(x) = 11.384 + 6.230x - 12.776x^2 \\ \quad \text{(FP- LAPW)} \end{cases} \tag{28}$$

$$\mathrm{Pb}_{1-x}\mathrm{Ca}_x\mathrm{Te} \Rightarrow \begin{cases} \varepsilon_1(x) = 11.585 - 2.522x - 0.8735x^2 \\ \quad \text{(from relation (21))} \\ \varepsilon_2(x) = 11.464 - 1.614x - 1.456x^2 \\ \quad \text{(from relation (22))} \\ \varepsilon_3(x) = 12.849 - 1.213x - 2.054x^2 \\ \quad \text{(from relation (23))} \\ \varepsilon_4(x) = 22.278 - 19.644x + 3.790x^2 \\ \quad \text{(FP- LAPW)} \end{cases} \tag{29}$$

where $\varepsilon_1(x)$, $\varepsilon_2(x)$, $\varepsilon_3(x)$ and $\varepsilon_4(x)$ stand for the optical dielectric constants estimated from the corresponding refractive indices $n_1(x)$, $n_2(x)$, $n_3(x)$ and $n_4(x)$, respectively, for a given value of x.

4. Conclusion

In summary, we have applied the FP-LAPW method in order to study the structural, electronic, thermodynamic and optical properties of $\mathrm{Pb}_{1-x}\mathrm{Ca}_x\mathrm{S}$, $\mathrm{Pb}_{1-x}\mathrm{Ca}_x\mathrm{Se}$ and $\mathrm{Pb}_{1-x}\mathrm{Ca}_x\mathrm{Te}$ ternary alloys. We have investigated the composition dependence of the lattice constant, bulk modulus, band gap, refractive index and dielectric function. The calculated lattice parameters for the three alloys exhibit a tendency to Vegard's law with a marginal bowing parameter. A small deviation of bulk modulus from LCD has been observed for all the three alloys. The physical origin of this effect should be mainly due to the weak mismatch of the bulk modulus of the binary compounds. The band structure was calculated by GGA. In addition, the EVGGA scheme has been used to obtain more accuracy. The bowing is found to be mainly caused by the charge-transfer effects, while the volume deformation and the structural relaxation contribute to the bowing parameter with a smaller magnitude. The investigation of the thermodynamic stability allowed us to calculate the critical temperatures for $\mathrm{Pb}_{1-x}\mathrm{Ca}_x\mathrm{S}$, $\mathrm{Pb}_{1-x}\mathrm{Ca}_x\mathrm{Se}$ and $\mathrm{Pb}_{1-x}\mathrm{Ca}_x\mathrm{Te}$ alloys, which are 425, 328 and 204 K, respectively.

Using the FP-LAPW method and empirical relations, the refractive index and the dielectric constant have been calculated as a function of composition x. The refractive index exhibits a nonlinearity, however, showing different bowing parameters, which arise from the effects of compositional alloy disorder. The same trend is observed for the dielectric constant.

References

[1] Masumoto K, Koguchi N, Takahashi S, Kiyosawa T and Nakatani I 1985 *Sci. Rep. Natl Res. Inst. Met.* **6** 101
[2] Shibata S, Horiguchi M, Jinguji K, Mitachi S, Kanamori T and Manabe T 1981 *Electron Lett.* **17** 775
[3] Koguchi N, Kiyosawa T and Takahashi S 1987 *J. Cryst. Growth* **81** 400
[4] Ishida A, Muramatsu K, Takashiba H and Eujiyasu H 1989 *Appl. Phys. Lett.* **55** 430
[5] Koguchi N and Takahashi S 1991 *Appl. Phys. Lett.* **58** 799
[6] Mochizuki K, Iwata Y, Isshiki M and Masumoto K 1991 *J. Cryst. Growth* **115** 687
[7] Jain C, Willis J R and Bullogh R 1990 *Adv. Phys.* **39** 127
[8] Albanesi E A, Peltzer E L, Blanca Y and Petukhov A G 2005 *Comput. Mater. Sci.* **32** 85–95
[9] Cohen M L and Chelikowsky J R 1989 *Electronic Structure and Optical Properties of Semi Conductors* (*Springer Series I Solid State Sciences* vol 75) 2nd edn (Berlin: Springer)
[10] Hinkel V, Hoak H, Mariana C, Sorba L, Horn K and Christensen N E 1989 *Phys. Rev.* B **40** 5549
[11] Zunger A, Wei S-H, Ferreira L G and Bernard J E 1990 *Phys. Rev. Lett.* **65** 353
[12] Blaha P, Schwarz K, Madsen G K H, Kvasnicka D and Luitz J 2001 *WIEN2k, an Augmented Plane Wave Plus Local Orbitals Program for Calculating Crystal Properties* Vienna University of Technology Vienna, Austria
[13] Perdew J P, Burke S and Ernzerhof M 1996 *Phys. Rev. Lett.* **77** 3865
[14] Engel E and Vosko S H 1993 *Phys. Rev.* B **47** 13164
[15] Murnaghan F D 1944 *Proc. Natl Acad. Sci. USA* **30** 5390
[16] Luo H, Greene R G, Handechari K G, Li T and Ruoff A L 1994 *Phys. Rev.* B **50** 16232
[17] Charifi Z, Baaziz H, El Haj Hassan F and Bouarissa N 2005 *J. Phys.: Condens. Matter* **17** 4083
[18] Lach-had M, Papaconstantopoulos D A and Mehl M J 2002 *J. Phys. Chem. Solids* **63** 833
[19] Madelung O, Schulz M and Weiss H (ed) 1983 *Numerical Data and Functional Relationships in Science and Technology* (*Landolt–Bornstein New Series* vol 17) (Berlin: Springer)
[20] Zaoui A and El Haj Hassan F 2001 *J. Phys.: Condens. Matter* **13** 253
[21] Vegard L 1921 *Z. Phys.* **5** 17
[22] Jobst J, Hommel D, Lunz U, Gerhard T and Landwehr G 1996 *Appl. Phys. Lett.* **69** 97
[23] El Haj Hassan F 2005 *Phys. Status Solidi* b **242** 909
[24] Dufek P, Blaha P and Schwarz K 1994 *Phys. Rev.* B **50** 7279
[25] Bachelet G B and Christensen N E 1995 *Phys. Rev.* B **31** 879
[26] Bernard J E and Zunger A 1986 *Phys. Rev. Lett.* **34** 5992
[27] Pauling L 1932 *J. Am. Chem. Soc.* **54** 3570
[28] Swalin R A 1961 *Thermodynamics of Solids* (New York: Wiley)

[29] Ferreira L G, Wei S H, Bernard J E and Zunger A 1999 *Phys. Rev.* B **40** 3197
[30] Teles L K, Furthmuller J, Scolfaro L M R, Leite J R and Bechstedt F 2000 *Phys. Rev.* B **62** 2475
[31] Gupta V P and Ravindra N M 1980 *Phys. Status Solidi* b **10** 715
[32] Ravindra N M, Auluck S and Srivastava V K 1979 *Phys. Status Solidi* b **93** 155
[33] Herve J P L and Vandamme L K J 1994 *Infrared Phys. Technol.* **35** 609
[34] Walton A K and Moss T S 1963 *Proc. Phys. Soc.* **81** 509
[35] Reddy R R, Nazeer Aharnmed Y, Abdul Azeem P, Rama Gopal K, Sasikala Devi B and Rao T V R 2003 *Def. Sci. J.* **53** 239
[36] Adachi S 1987 *J. Appl. Phys.* **61** 4869